DESIGN AND OPTIMIZE A TWO COLOR FOURIER DOMAIN PUMP PROBE

OPTICAL COHERENCE TOMOGRAPHY SYSTEM

A Thesis

by

DESMOND JACOB

Submitted to the Office of Graduate Studies of
Texas A&M University
in partial fulfillment of the requirements for the degree of

MASTER OF SCIENCE

May 2009

Major Subject: Biomedical Engineering

DESIGN AND OPTIMIZE A TWO COLOR FOURIER DOMAIN PUMP PROBE

OPTICAL COHERENCE TOMOGRAPHY SYSTEM

A Thesis

by

DESMOND JACOB

Submitted to the Office of Graduate Studies of
Texas A&M University
in partial fulfillment of the requirements for the degree of

MASTER OF SCIENCE

Approved by:

Chair of Committee,	Brian E. Applegate
Committee Members,	Alvin T. Yeh
	Arum Han
Head of Department,	Gerard L. Cote

May 2009

Major Subject: Biomedical Engineering

ABSTRACT

Design and Optimize a Two Color Fourier Domain Pump Probe Optical Coherence

Tomography System. (May 2009)

Desmond Jacob, B.E., University of Pune, India

Chair of Advisory Committee: Dr. Brian E. Applegate

Molecular imaging using fluorescence spectroscopy-based techniques is generally inefficient due to the low quantum yield of most naturally occurring biomolecules. Current fluorescence imaging techniques tag these biomolecules chemically or through genetic manipulation, increasing the complexity of the system. A technique capable of imaging these biomolecules without modifying the chromophore and/or its environment could provide vital biometric parameters and unique insights into various biological processes at a molecular level.

Pump probe spectroscopy has been used extensively to study the molecular properties of poorly fluorescing biomolecules, because it utilizes the known absorption spectrum of these chromophores. Optical Coherence Tomography (OCT) is an optical imaging modality that harnesses the power of low coherence interferometry to measure the 3-D spatially resolved reflectivity of a tissue sample. We plan to develop a new molecular imaging modality that combines these techniques to provide 3-D, high-resolution molecular images of various important biomolecules.

The system uses a Fourier domain OCT setup with a modified sample arm that combines the "pump" and "probe" beams. The pump beam drives the molecules from the ground state to excited state and the probe interrogates the population change due to the pump and is detected interferometrically. The pump and the probe beam wavelengths are optimized to maximize absorption at the pump wavelength and maximize the penetration depth at the probe wavelength. The pump-probe delay can be varied to measure the rate at which the excited state repopulates the ground state, i.e., the ground state recovery time. The ground state recovery time varies for different chromophores and can potentially be used to identify different biomolecules.

The system was designed and optimized to increase the SNR of the PPOCT signals. It was tested by imaging hemoglobin and melanin samples and yielded encouraging results. Potential applications of imaging hemoglobin using this technique include the mapping of tissue microvasculature and measuring blood-oxygen saturation levels. These applications could be used to identify hypoxic areas in tissue. Melanin imaging can provide means of demarcation of melanoma in various organs such as skin, eye and intestines.

To my parents

ACKNOWLEDGEMENTS

I would like to thank my committee chair, Dr. Brian Applegate, and my committee members, Dr. Alvin Yeh, and Dr. Arum Han, for their guidance and support throughout the course of this research.

Thanks also go to my friends and the department faculty and staff for making my time at Texas A&M University a great experience. I would like to thank my lab mates in a big way for their contributions and advice. This project was partly funded through the National Institutes of Health and I extend my gratitude for their support.

Last but not the least, I thank my parents and brother for their constant support and encouragement.

TABLE OF CONTENTS

LIST OF FIGURES

1. INTRODUCTION

Molecular imaging is a technique that unites molecular biology and *in vivo* imaging. Since all diseases originate on the molecular and cellular levels, there is a need to better understand the molecular pathways inside an organism noninvasively. Molecular imaging provides access to the biochemical makeup and biochemical processes occurring on the molecular and cellular levels. For instance: protein-protein interactions, cell signal transduction, gene expression and gene delivery, etc. Molecular imaging could help elucidate the cause, progression and diagnosis of diseases such as cancer and neurological disorders, leading to improved treatment of these diseases by optimizing clinical trials of new drugs and procedures. Non-invasive molecular imaging also allows longitudinal animal studies by reducing the animal count and error from inter-individual variability.

Molecular imaging relies on targeting specific biomarkers or chromophores to study the biological pathways and processes. These biomolecules could either be naturally occurring or artificial markers that interact with target chromophores. This approach in imaging is vitally different from traditional imaging principles that rely on differences in contrast or water content in an image. This increases the specificity of the imaging modality, i.e., the ability to distinguish between different chromophores. Many

_____

This thesis follows the style of *Optics Express.*

emission computed tomography (SPECT) and Fluorescence-based optical imaging have been recently developed. These techniques have been used for obtaining high resolution images but each technique has its strength and weaknesses.

Fluorescence-based imaging techniques, for example, have become increasingly popular for obtaining high resolution 3-D images at a molecular level. However, the complex biological environment provides numerous pathways to release the absorbed energy with greater efficiency. This results in only a small percentage of biomolecules that fluoresce efficiently, rendering a large number of important biomolecules inaccessible to fluorescence-based molecular imaging techniques. To overcome this limitation these poorly fluorescing biomolecules are tagged chemically or through genetic manipulation by fluorescent markers. This not only increases the complexity but could also interfere with the process under study [1].

These drawbacks have been successfully overcome in pump-probe spectroscopy techniques and have been used extensively for measuring the molecular properties of poorly fluorescing biomolecules. We intend to use this technique with optical coherence tomography (OCT) to obtain high resolution 3-D optical molecular images of biological systems. OCT is an emerging optical imaging modality capable of providing micrometer (3-20 μm) scale images in highly scattering media at depths of 1-2 mm. This new high resolution 3-D optical molecular imaging technique is capable of probing a large number of poorly fluorescing biomolecular species. In this project, we have developed a two–color, pump-probe optical coherence tomography (PPOCT) system. This system was

tested on commonly occurring biological chromophores such as hemoglobin and melanin.

Fluorescence spectroscopy-based techniques cannot image oxy- or deoxy-hemoglobin effectively as these are very poor fluorophores. Effective imaging of these chromophores would enable us to map the tissue microcirculation; including blood oxygen saturation and flow, which provide insight into the mechanisms of many diseases. The most obvious are cardiovascular diseases where it has been noted that "… functional abnormalities of the microcirculation are one of the primary abnormalities in cardiovascular disease pathogenesis …" [2]. Damage to microcirculation has been implicated in inflammatory diseases such as Crohn's disease [3] and acute pancreatitis [4]. It has also been well established that angiogenesis is an important factor in tumor metastasis, both for the growth and spread of the primary tumor to distant sites and the subsequent growth of secondary tumors at those sites [5, 6]. Moreover, blood oxygen saturation is an important biometric in microvasculature for tumor growth and response to treatment [7], ischemia/reperfusion [8] and wound healing [9].

Melanin is an abundant endogenous pigment with a poorly understood molecular structure. There are two basic forms, eumelanin (black) and pheomelanin (red). Both have a broad absorption spectrum stretching from the UV to the near IR. Melanoma is a malignant tumor of the melanin producing melanocytes found in the skin, intestine, and eye. Intraocular melanoma involves occurrence of malignant cells in the various tissues of the eye such as the iris, ciliary body and choroid. Since melanoma is an aggressive cancer, early diagnosis is extremely important to prevent the spread of the cancer and to

preserve vision in the afflicted eye. The excited state dynamics of melanin have been extensively investigated using pump-probe spectroscopy [10]. The dynamics indicate the presence of both short (picosecond) and long (nanosecond) lifetime states which may be used for the detection of transient absorption via PPOCT.

A non-invasive imaging modality such as PPOCT that is capable of making detailed 3-D maps of oxy/deoxy hemoglobin and melanin could prove to be an invaluable tool for studying various diseases in animal models. It may also have clinical value for diagnosis and monitoring of these diseases.

2. THEORY

Optical Coherence tomography (OCT) is a high resolution, optical imaging technique that allows micron scale tomographic sectioning of biological samples over small distances [11, 12]. OCT measures the backscattered light from a surface and provides subsurface imaging with high spatial resolution (~5-10 μm) in three dimensions. OCT is based on the one dimensional technique of optical low coherence reflectometry (OLCR) which uses a Michelson's interferometer to measure the back reflected light. In OLCR the interference fringes occur when the optical pathlengths of the sample and reference beams match within the coherence length. The coherence length for a Gaussian source is given by:

$$l_c = \frac{2 \ln 2}{\pi} \frac{\lambda^2}{\Delta\lambda} \tag{1}$$

Here, l_c is the coherence length, λ is the mean wavelength of the source, $\Delta\lambda$ is the full width half maximum (FWHM) of the source. The depth in the sample corresponds to the difference in optical path lengths between a known reference beam and reflecting/scattering sites in the sample, and that of a known delay. A series of adjacent depth scans are then processed to produce a 3-D cross-sectional image.

The axial resolution of the OCT system is limited by the coherence length of the illumination, while the lateral resolution is determined by the diameter of the focused spot size in the sample. Thus, the lateral resolution is decoupled from the axial resolution, which results in excellent depth resolution even at sites that are not accessible

by high numerical aperture (NA) beams. The coherence lengths for typical OCT light

sources are ~10 μm, with ultra-broad band sources extending this to the region of 1 μm,

providing cellular and subcellular resolution, respectively. The imaging depth for light

sources in the near infrared region of the spectrum is ~1-2 mm. Moreover, the

interferometric technique provides high dynamic range and sensitivity (> 110 dB). A

typical time domain OCT system is depicted in figure 1. In this system, the

interferometric signal is isolated from one depth at a time as the reference mirror is

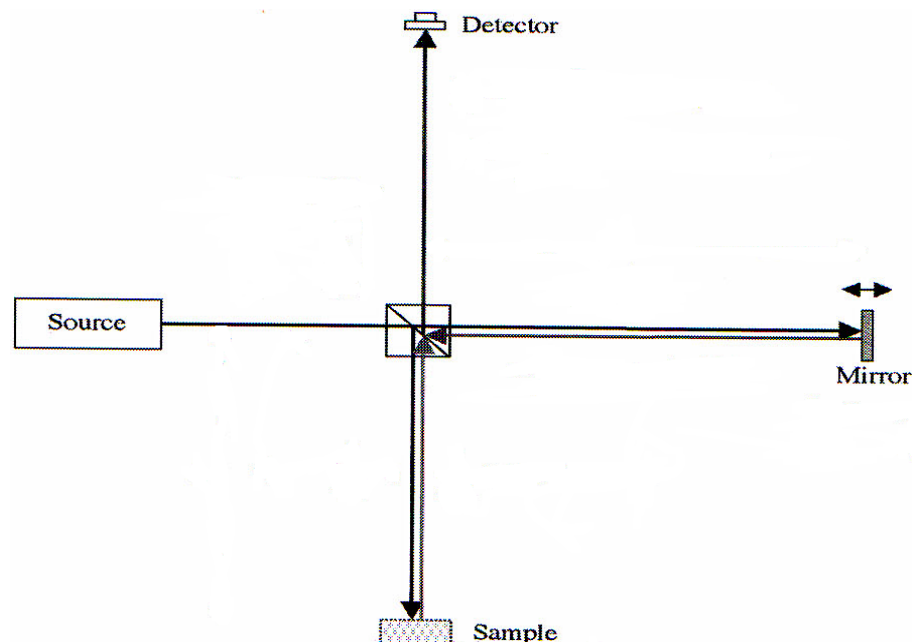scanned over the coherence length of the source.

Figure 1. Michelson interferometer-based OCT system. A coherent light source, such as a laser,

is used as the source. A beamsplitter sends the light to the sample and the reference arm. The

reflected light from the sample and the reference mirror interfere at the detector.

The time domain OCT system depicted in figure 1 has been successfully used in a majority of biological and medical applications. However an alternate technique for collecting OCT signals from a sample has been shown to improve the signal to noise ratio (SNR) and reduce the system complexity. In this method the interferometric signal is collected as a function of optical wavenumber. This is done either by using a Fourier domain OCT (FDOCT) [13-15] technique or swept source OCT (SSOCT) [16-19] technique. A FDOCT system uses a broadband light source and the interferometric signal is sent to a dispersive spectrometer in the sample arm to achieve spectral separation. This signal is then collected by high speed detector and processed to obtain depth resolved scans. In a SSOCT system, however, a tunable narrowband source is used to illuminate the sample over a broad optical bandwidth and the optical wavenumber is time encoded with the tuned wavelength. Both these methods have shown an improvement of 15-20 dB over time domain OCT systems. A block diagram of FDOCT system employing an optical fiber coupler-based interferometer is depicted in figure 2.
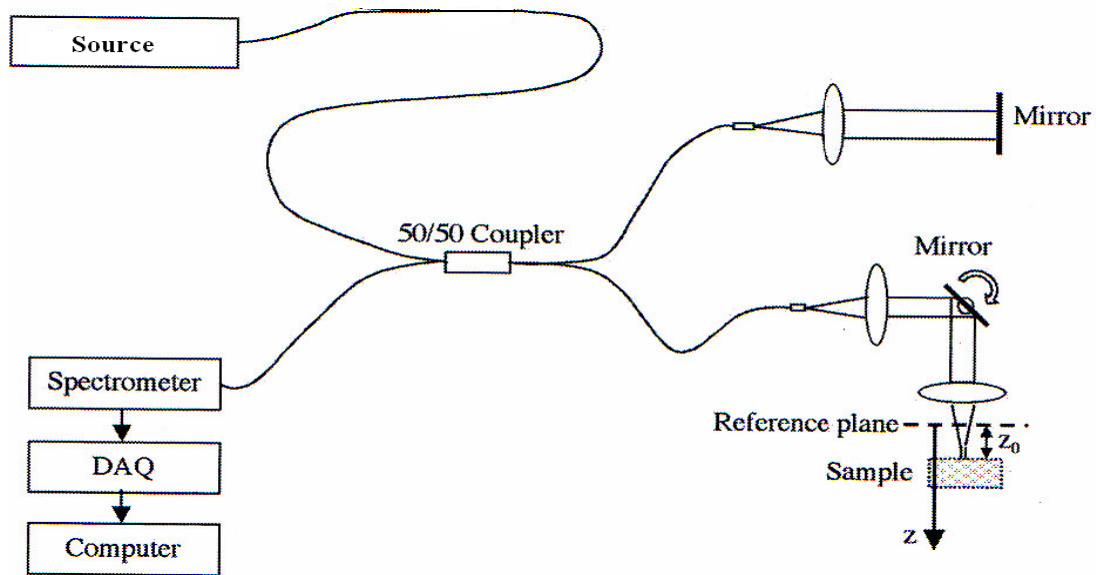
Figure 2. FDOCT system employing a fiber coupler-based interferometer. The scanning mirror in the sample arm is used to scan the sample to obtain a 3D image.

In spite of its advantages in terms of high lateral and axial resolution and sensitivity, a standard OCT system does not inherently have the ability to measure molecular signatures essential for molecular imaging. This is because the scattering cross-section that gives rise to the intrinsic tissue reflectivity does not vary much between different molecular species. This limitation was overcome by adapting OCT to a number of molecular spectroscopic techniques, including pump-probe [20, 21], second harmonic generation [22-24], coherent anti-Stokes Raman scattering [25], and linear absorption [26] to provide molecular contrast, with varying degrees of success. Molecular specificity in OCT imaging can also be introduced by modifying the tissue scattering properties. The introduction of molecular aggregates [27], engineered

microspheres [28] and gold nanoparticles [29] to OCT systems have been used to increase molecular specificity.

In this project we have combined pump-probe spectroscopy techniques with OCT. Pump-probe spectroscopy has been established as a useful tool for imaging chromophores that are inefficient fluorophores. Important biomolecular species such as deoxyribonucleic acid (DNA), ribonucleic acid (RNA), oxy and deoxy hemoglobin and nicotinamide adenine dinucleotide (NAD^+) are largely invisible to fluorescence-based techniques because of their poor quantum yield. However, if imaged, these biomolecules would provide access to a number of physiological processes occurring in the biological tissues such as metabolism, mitosis and oxygen transport. Each of these biomolecules has a known absorption spectrum which can be utilized for molecular imaging using pump-probe spectroscopy.

We employ a pump-probe technique that is designed to measure the change in the ground state population of the target chromophore. This technique is likely to give a better sensitivity than techniques which try to measure changes in the excited state population of the chromophore [30]. A representation of the basic principle of this technique is shown in figure 3. Two laser pulses, the pump and probe, are applied on the sample with a time delay t_d. The pump pulse drives the ground state population to excited state and the probe interrogates the change induced by the pump by measuring the net difference in the probe attenuation with and without the pump pulse. This attenuation is directly proportional to the net change in the ground state population.
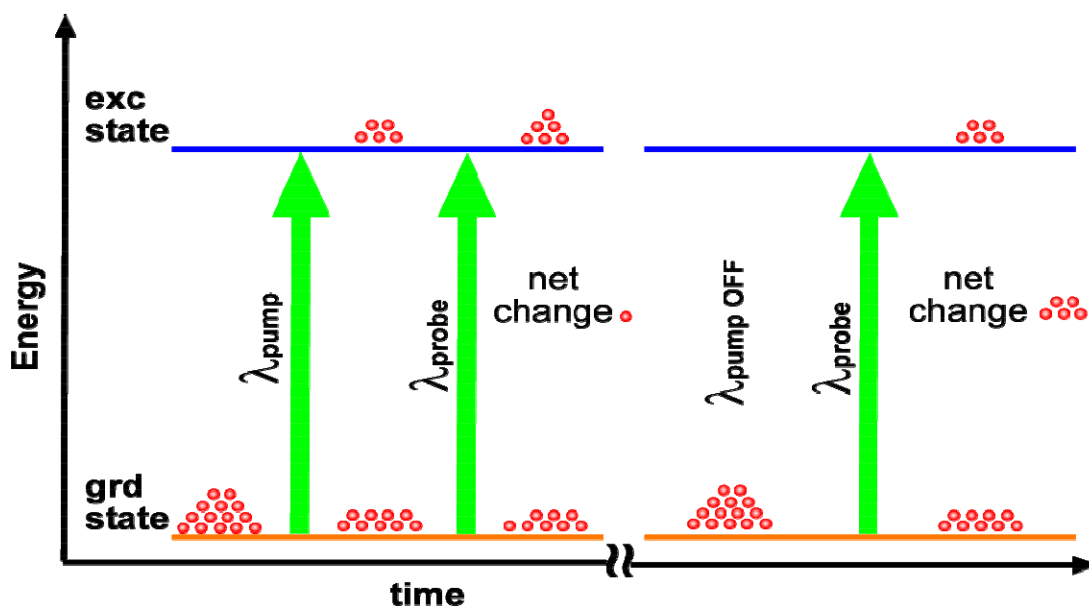
Figure 3: Energy level diagram of a ground state recovery pump-probe experiment. The pump radiation transfers ground state population into the excited state. The probe radiation then measures the population transfer induced by the pump, which is manifested as a reduction in ground state absorption [31].

This pump-probe based technique yields two important molecular properties that contribute to molecular specificity. The magnitude of the transient absorption can be measured as a function of wavelength. Since only those states connected by both the pump and probe contribute to the signal, this maps the absorption spectrum of the chromophore. Another molecular property that further improves the specificity is the ground state recovery (gsr) time. This is the time required for the molecules in the excited state to spontaneously relax back to the ground state. The gsr time is calculated by measuring the magnitude of the transient absorption at various pump-probe delay times, and indicates the molecular chromophore, as well as its local environment.

A simple realization of pump probe OCT was successfully implemented

previously called the ground state recovery Pump Probe Optical Coherence Tomography

(gsrPPOCT) [31]. This system used a time domain OCT system with degenerate pump

and probe pulses at 530 nm from a Nd:Glass, femto-second pulsed laser. The equations

describing the signal to noise ratio of this single color gsrPPOCT system have been

derived previously in reference [30]. A summary of the results of the derivation is given

below. The predicted gsrPPOCT *SNR* for a model two level molecular system is given

by:

$$SNR = \frac{R\rho P_{pr}}{2Be} e^{-2\sigma 1\,(N1(t)-N2(t))z}$$

Where,

$$N1(t) - N2(t) = N1^0 \left[1 - \exp\left(\frac{-2\sigma 1\,\lambda_{pu}P_{pu}\cos^2(\omega t)}{hc\pi r^2}\right)\right]$$

And

$$SNR \approx \frac{R\rho P_{pr}}{2Be} \left(\frac{\sigma 1^2 z N_1{}^0 \lambda_{pu}P_{pu}}{hc\pi r^2 f_0}\right)^2$$

where R is the sample reflectivity, ρ is the detector responsivity, P_{pr} is the sample arm

power in the OCT interferometer, B is the detection bandwidth, e is the electron charge,

f_0 is the laser pulse repetition rate, $N_1(t)$ and $N_2(t)$ are the time dependent ground and

excited state populations integrated over the pump pulse duration, N_{10} is the ground

state population before interacting with the pump laser, σ_1 is the absorption cross

section, z is the absorption path length, λ_{pu} is the pump wavelength, P_{pu} is the average

pump power, ω is the pump modulation frequency, h is Planck's constant, c is the speed of light, and r is the focal spot radius. The final approximation is a result of assuming weak absorption of the pump and probe beams where the exponential function may be approximated by the first two terms of its Taylor series expansion.

The gsrPPOCT system was more efficient than previous pump-probe OCT techniques because it measured the transient absorption on very short time scales before processes such as spontaneous emission were able to depopulate the state. This system was optimized to about 6dB of the theoretical SNR and had a projected penetration depth of around 570μm – 1000 μm. It was successfully used for *in situ* imaging of two different chromophores; transfectable protein dsRed and the protein hemoglobin. However there were several shortcomings of the degenerate gsrPPOCT techniques that we have attempted to address in this project.

The penetration depth of the gsrPPOCT system was limited by the strong scattering at the short wavelength used for imaging (530 nm). A two color pump probe system would allow us to move the probe wavelength to lower wavelengths (Near IR/ IR) where the tissue's light scattering properties are more favorable, while keeping the pump wavelength in the visible region where the absorption cross section of most biomolecules is relatively high. The projected penetration depth in the IR region for the probe is expected to be in the range of 800 μm to 1200 μm.

The gsrPPOCT system was based on a time domain OCT system. Moving to a Fourier domain OCT system would improve our sensitivity by a factor of 100. The use of a Fourier domain OCT system would also increase the imaging speed, which was

limited to ~1 Hz in the gsrPPOCT system, by trading some of the sensitivity for higher imaging speed. Additionally, the gsrPPOCT system was pumped and probed at the same wavelength. By moving to two different wavelengths for the pump and probe pulses, the system will utilize two electronic transitions. This would require the molecular chromophore to have absorption at both wavelengths to produce a signal, thereby increasing the specificity.

3. DESIGN

The proposed system is based on a Fourier domain OCT technique because it offers better sensitivity. A simple representation of the proposed pump-probe OCT (PPOCT) system is depicted in figure 4. This section will discuss the design and implementation of each of these stages in detail.
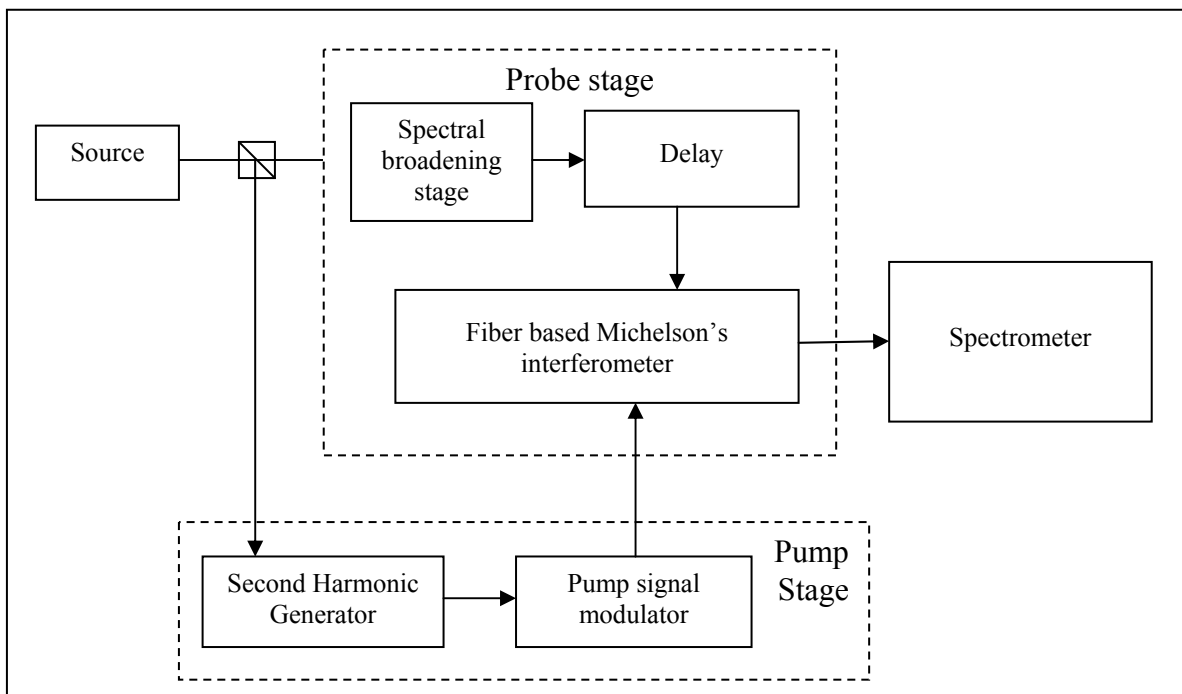
Figure 4: Block representation of the proposed PPOCT system.

3.1 Fourier Domain Optical Coherence Tomography

Fourier domain optical coherence tomography (FDOCT), just like the conventional time domain OCT, uses a broadband light source. However, unlike TDOCT, the reference mirror is not scanned in the z axis to obtain the depth information. The depth information in FDOCT is obtained by evaluating the interference spectrum that is collected on a detector array such as a charge coupled device (CCD). The Fourier transform of the interferogram provides the back reflection intensity as a function of depth. The depth information is then obtained from the spectrally resolved interference signal that arises from different pathlengths in the sample and reference arm. This spectral intensity at the detector of an interferometer is represented by the following equation.

$$I_D = I_S + I_R + 2\,\text{Re}\,(\gamma_{11(z)})\,\sqrt{I_S\,I_R}\,\cos(2k\Delta z)$$

Here, I_R and I_S are the irradiance due to electric field of reference beam and represents the DC component of irradiance. The third term is the actual interference signal, $\gamma_{11(z)}$ represents the degree of coherence. Its real part has a value from 0 to 1. The value of the degree of coherence can be classified as $|\gamma_{11(z)}| = 1$; Coherent limit; $|\gamma_{11(z)}| = 0$; Incoherent Limit; $0 < |\gamma_{11(z)}| < 1$ Partial coherence.

3.2 Source

We use a femtosecond Ti:Sapphire laser that has a tunable range from 680 nm to 1080nm with a repetition rate of 80 MHz as a source. The narrow band (~5nm) signal

was sent through a single mode fiber for spectral broadening to provide an axial resolution of 10-12nm. The center frequency of the laser was optimized for sensitivity to hemoglobin. Figure 5 shows the absorption spectrum of oxy- and deoxy- hemoglobin. The figure below shows a sharp absorption peak at around 415nm. In order to utilize this peak, we chose our center wavelength of 830nm for the probe pulse. The pump wavelength of 415nm was obtained though second harmonic generation using a beta-BaB_2O_4 (BBO) crystal.
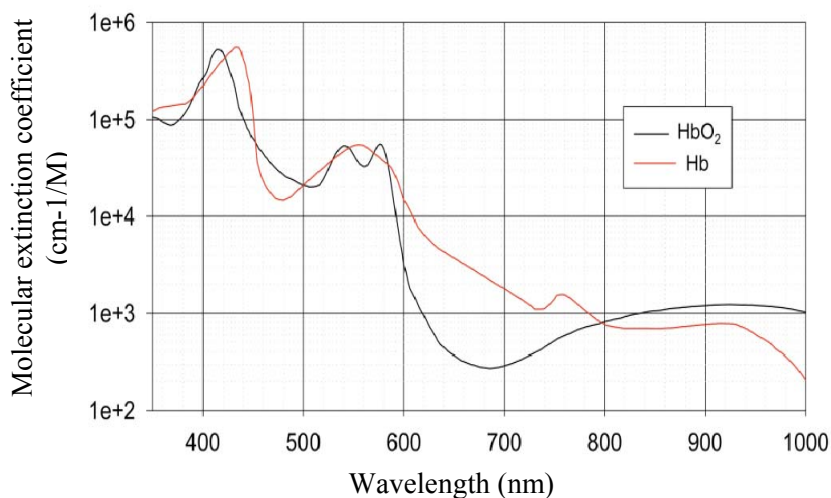

Figure 5: Absorption spectrum of oxy and deoxy hemoglobin [33].

3.3 Spectral broadening

OCT relies on a broad spectral source for imaging as there is a Fourier relationship between the auto correlation of a stationary random process and the power spectrum of the process. Thus, a narrow source spectrum leads to a very long coherence length and a broad axial resolution, while a broad source spectrum leads to a narrow

point spread function. Therefore, it is imperative that the narrow spectrum from the laser be broadened to give a better axial resolution.

We used single mode fiber of an approximate length of 1m to broaden the spectrum. The spectral broadening was obtained through self phase modulation of the laser pulses once coupled into the single mode fiber. This method of broadening has been shown to significantly improve the resolution of an OCT system over methods that use nonlinear microstructure fibers (MSF) to obtain broadening [32]. MSF's are extremely sensitive to pulse energy and could thus severely limit an OCT system's signal to noise ratio (SNR) which is a function of the intensity noise of the source.

We experimented with three types of single mode fibers for our application. A polarization maintaining single mode fiber (PM fiber) was initially used for spectral broadening. However, this resulted in the generation of sidebands in the OCT signal. This broadened the axial point spread function thereby reducing the axial resolution of the system significantly. We then tried out a high numerical aperture (NA) single mode fiber (NA = 0.35) and compared it with a simple single mode fiber (NA = 0.1 to 0.14). We found that the broadening from a normal fiber was comparable to that from the high NA fiber for the same source power. We therefore decided to use the normal fiber since these are inexpensive and easier to obtain. A half-wave plate was introduced before the fiber launching stage for adjusting the polarization of the light going in the fiber so that it gave a smooth output spectrum after broadening.

3.4 Pump signal modulator and second harmonic generation

The pump signal was frequency encoded to separate the PPOCT signal from the acquired interferogram. Some of the most common techniques used to modulate a laser beam are by the use of either an electro-optic modulator (EOM), an acousto-optic modulator (AOM), or an optical chopper. We began using the optical chopper for initial measurements of signal from hemoglobin (Hb); however, the chopper limited the maximum modulation frequency to 6 KHz. An analysis of the noise spectrum for our system shows that the random intensity noise was more pronounced at frequencies closer to DC. Thus a limitation of 6 KHz meant that the modulation frequency was more susceptible to random intensity noise.

The AOM and the EOM have a maximum range of up to 100 KHz. The AOM uses a diffraction grating to modulate a beam by switching the beam between the 0th and 1st order. However this grating also results in slight spectral broadening of the beam. A spectrally broadened beam such as this is known to produce an elliptical shaped frequency doubled beam when used for second harmonic generation using a non linear crystal. An elliptical beam is unsuitable for our application. Therefore, we used a commercially available EOM from Thorlabs® (EO-AM-NR-C1). The modulation signal for the EOM was generated by the LabView® code. This code also processed the PPOCT signal and supplied the signal to the EOM amplifier which was used to drive the EOM.

The pump pulse for the system was generated using frequency doubling by focusing the 830 nm light from the laser on to a BaB_2O_4 (BBO) crystal. The crystal was

mounted on a rotating mount and the angle for second harmonic generation was set by hand.

3.5 Delay

The pump and the probe pulse pump-probe system are typically separated by a small, finite delay. We create this delay by introducing an adjustable delay stage in the probe arm, then matching the lengths of the pump and probe arms. The delay is fashioned out of right angled prisms mounted on translation stage. The maximum delay that can be set is limited by the physical length of the translation stage and the delay between subsequent pump pulses (12.5 ns in our case). However, this limitation is not significant, as most poorly fluorescing biomolecules have excited state lifetime within this range. The excited state dynamics of melanin have been widely studied [10], but those of hemoglobin at our wavelength of operation haven't been explicitly reported. The studies indicate that melanin has both a short (picosecond) and long (nanosecond) excited state lifetime which can be used for PPOCT.

We conducted a series of pump probe transient absorption experiments to study the effect of delay on the strength of pump probe signal. The optical setup used is shown in figure 6. We used the Ti:Sapph as the source and split the output beam into a pump and probe beam using the beam splitter. The pump beam was modulated using the EO and the BBO crystal was used to obtain the frequency doubled pump beam at 415 nm. The probe was sent to polarizing beam splitter (PBS) and the reflected beam was directed on to a mirror mounted on a translation stage. A quarter waveplate was placed

between the PBS and this mirror so that the reflected beam coming back to the PBS would be cross polarized to the incident beam and would hence propagate straight through and onto a mirror. The pathlength of the pump and probe beam combining at the PBS was matched using the mirror mounted on the translation stage.
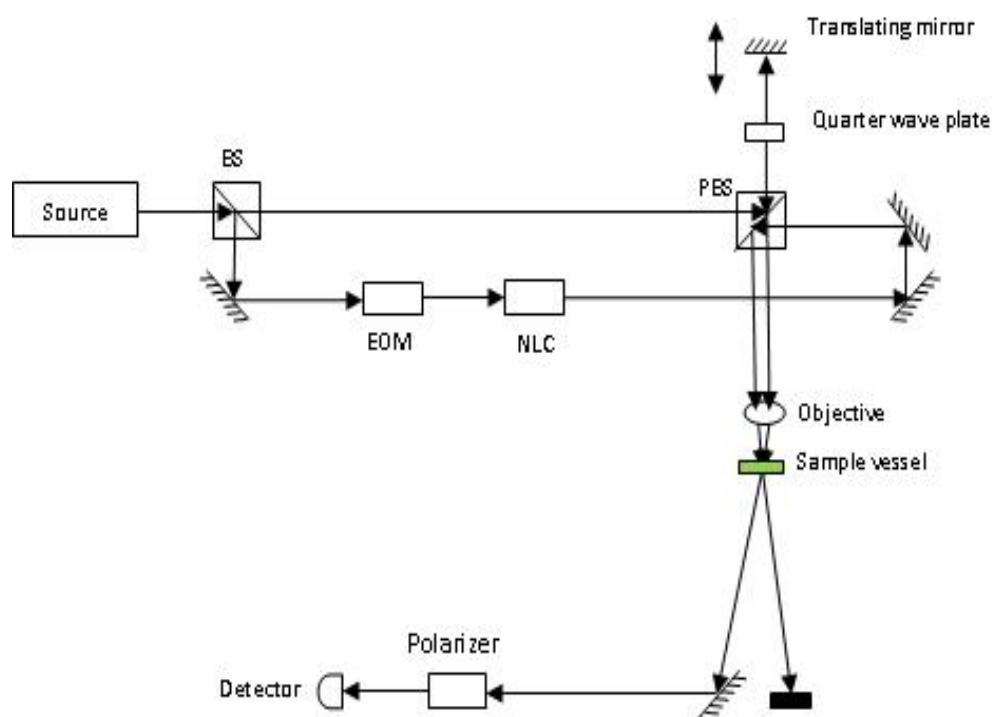

Figure 6: Schematic of Pump probe transient absorption experiment setup. Abbreviations: BS beam splitter, EOM Electro-optic Modulator, NLC Non-Linear Crystal, PBS polarizing beam splitter.

The combined pump and the probe were aligned such that they travelled parallel to each other, and were incident on a focusing lens. This lens was mounted in a way such that the pump and the probe overlapped only at the sample. The two beams diverged

beyond the sample and were spatially filtered. The probe beam was then directed to a detector and recorded. Further filtering of the probe beam was achieved by using a polarizer near the detector to prevent any bleed-through of the pump signal. The signal collected by the detector is filtered around the pump modulation frequency and recorded.

This setup was used to measure the pump-probe trans-absorption signal from Indocyanine Green (IcG) and hemoglobin solutions. IcG is a commercially available dye that is extensively used in ophthalmology as an intravascular dye. It has a well-defined absorption spectrum that can be used for PPOCT applications. The pump and probe wavelengths were set at 780 nm for the set of experiments carried out on IcG as IcG exhibits a sharp absorption peak at this wavelength. However, the pump and probe wavelengths for the hemoglobin sample were set to 415 nm and 830 nm, respectively. The delay was set by moving the mirror mounted on the translation stage.

A 60 µM solution of IcG in Methanol (anhydrous, 99.8%) was used as the sample solution. This solution was held in a 1mm pathlength cuvette and placed at the focal point of the two beams. The hemoglobin sample solution was prepared from ferrous stabilized human hemoglobin acquired from Sigma Aldrich® with a molarity of 500 µM. The reference mirror was moved over a region corresponding to -2 ps to 6.3 ps at 600 fs steps. The resulting pump probe trans-absorption signal was recorded to identify any peaks corresponding to a discernable ground state recovery time. While the results suggest that there might be a short lifetime state (2-4 ps region) for IcG, the same could not be asserted with hemoglobin. The signal strength from the Hb sample remained largely same over the entire delay range. We attribute the strong signal from

the Hb sample to large lifetime(s) (> 12.5 ns), however the existence of very short

lifetimes (<500 fsec) could not be ruled out because to the limitation on the temporal

resolution of the laser pulses. We therefore concluded that the delay between the pump

and probe signal was not critical as long as the pump pulse always lead the probe by

more than a few tens of picoseconds.

3.6 OCT interferometer

The interferometer was built around a 50/50 fiber coupler. The probe pulse

coming out of the delay stage was launched into one of the input arm of the coupler and

the two output arms were used for the sample and reference arms of the interferometer.

The pump beam was combined with the probe beam using a dichroic mirror (DM)

placed in the sample arm. The combined beam was then directed onto a pair of scanning

galvanometer mirrors which sent the beam through the focusing lens onto the sample.

The back reflected light was collected and sent to the spectrometer placed in the detector

arm of the interferometer.

3.7 Spectrometer

A spectrometer is a critical component of a FDOCT system. A custom-built high

speed spectrometer was placed in the detection arm of the OCT interferometer. It

consisted of a 2" collimation lens which guided the beam coming out of the detector arm

of the interferometer to a dispersive grating. The resultant diffracted beam was then

focused on the fast line-scanning camera using a compound lens. An Atmel AViiVA™

in line fast scanning camera (AViiVA™ M2 CL 2014) was used at the detector. The

camera has 2048 pixels with 14 μm pitch and is capable of a maximum line rate of 28

kHz. The spectrometer was calibrated using the atomic lines from an argon lamp.

The axial imaging range of FDOCT according to the Fourier relationship is

limited by the fringe visibility degradation with increasing imaging depth. This is called

the fall off. The spectral range integrated by each pixel along with the optical resolution

of the spectrometer determines the fall off. In other words, the fall off is a convolution of

a rectangular function corresponding to the width of a pixel and the coherence length of

the interferometric signal. The fall off for the spectrometer is determined by measuring

the one-sided depth corresponding to a loss of 3 dB in the sensitivity of the signal. Fall

off can be improved by optimizing the spectrometer design and careful system

alignment. The fall off for our spectrometer is ~800 μm.

3.8 Data acquisition and processing

The spectrometer output is acquired through a camera link card and processed

using LabView®. The following algorithm is then employed to acquire the PPOCT

signal from the recorded M-scan. The OCT A-lines from the M-scan are transformed

into k-space, resampled, and a fast Fourier transform is done to obtain an A-line. A

Fourier transform is then performed at each depth of the M-scan along the time axis. The

magnitude of this signal is then filtered around the pump modulation frequency and

integrated. Each depth resolved integrated point corresponds to one pixel in the PPOCT

A-Line.

Figure 7 shows the schematic of the system. For initial testing and signal acquisition from hemoglobin an optical chopper was used in place of the EOM.
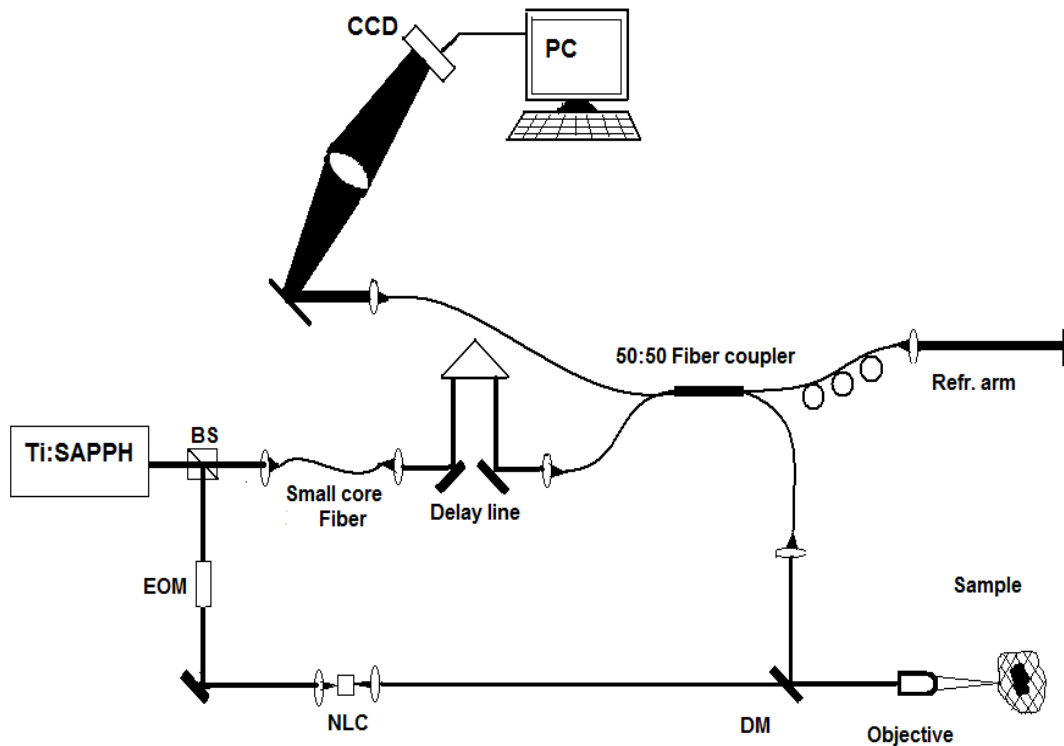

Figure 7: Schematic of the PPOCT system. Abbreviations: BS beam splitter, EOM Electro-optic Modulator, NLC Non-Linear Crystal, DM Dichroic Mirror, Ti:Sapph Ti:Sapphire laser source and CCD charge coupled device.

4. RESULTS AND DISCUSSION

The OCT system was built first and the SNR was optimized. The OCT system had an axial resolution of ~8 μm and a lateral resolution of ~14 μm. The integration time was set to 30 μsec and the corresponding SNR was measured to be around 100 dB for an incident power of 1.4 mW on the sample. The OCT system was used to obtain cross sectional images of human arteries and mouse cochlea, among other things. Figure 8 shows cross sectional images of mouse cochlea.*

The images were collected at 830 nm with a sample power of around 2.5mW and an integration time of 50 μsec. The galvanometer mirrors were used to scan the beam by 4 mm in the x-direction and 2mm in the y-direction to obtain the cross sectional images at steps of 400 μm in the y-direction. The raw data was collected and processed in the standard way. Spatial filtering was then applied to boost the SNR by convolving the image with a 2-D Gaussian profile that had a standard deviation of 3.5 pixels (~4 microns/pixel). The figure below includes four such cross sectional images that were collected from the cochlea.

_____

* The mouse cochlea were harvested and fixed by Dr. John S. Oghalai's group at the department of Neuroscience at Baylor College of Medicine, Houston.
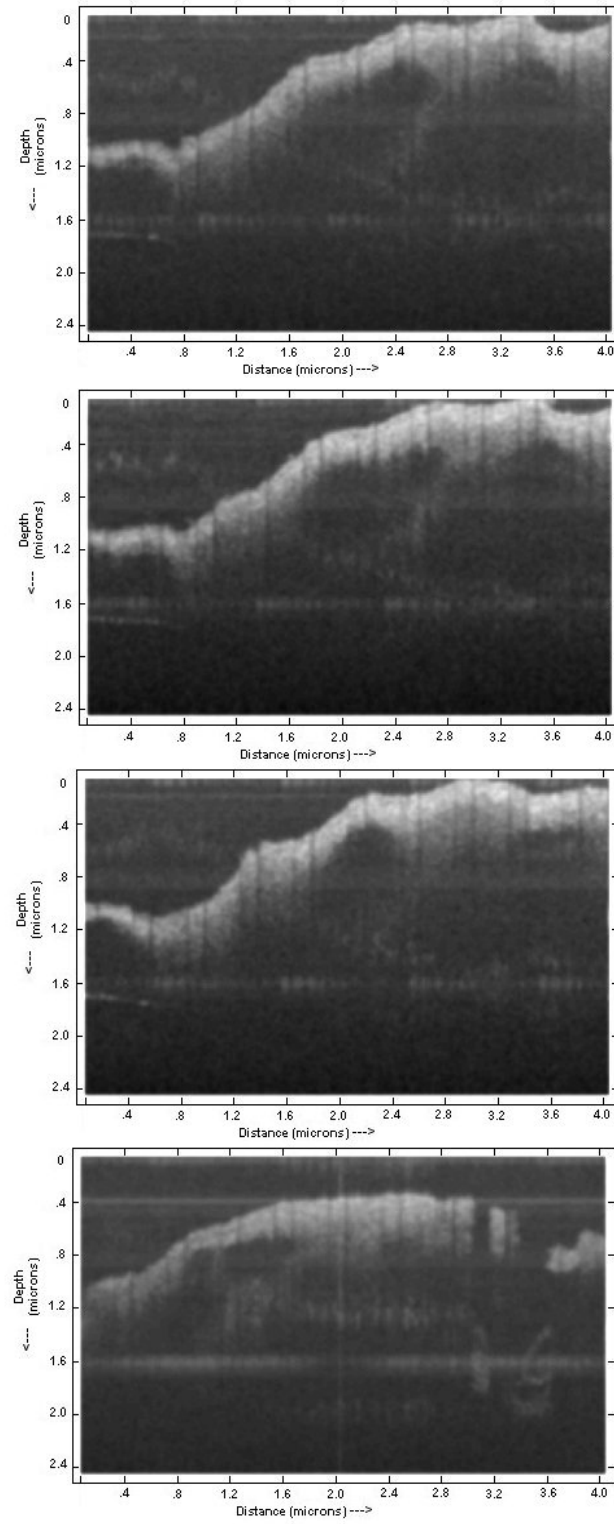
Figure 8: Cross sectional images of mouse cochlea.

Once the pump beam was integrated with this system, we began the process of tuning and optimizing the system to acquire PPOCT signals. The system was tested on a sample of pure hemoglobin that was placed in a custom built sample vessel. The sample vessel was constructed by placing a droplet of ~800 µM aqueous hemoglobin solution between two coverslips and allowing it to dry. The optical pathlength through the hemoglobin solution was determined to be ~18 µm based on the OCT measurements. A typical OCT and PPOCT A-line recorded using this sample is shown in figure 9.
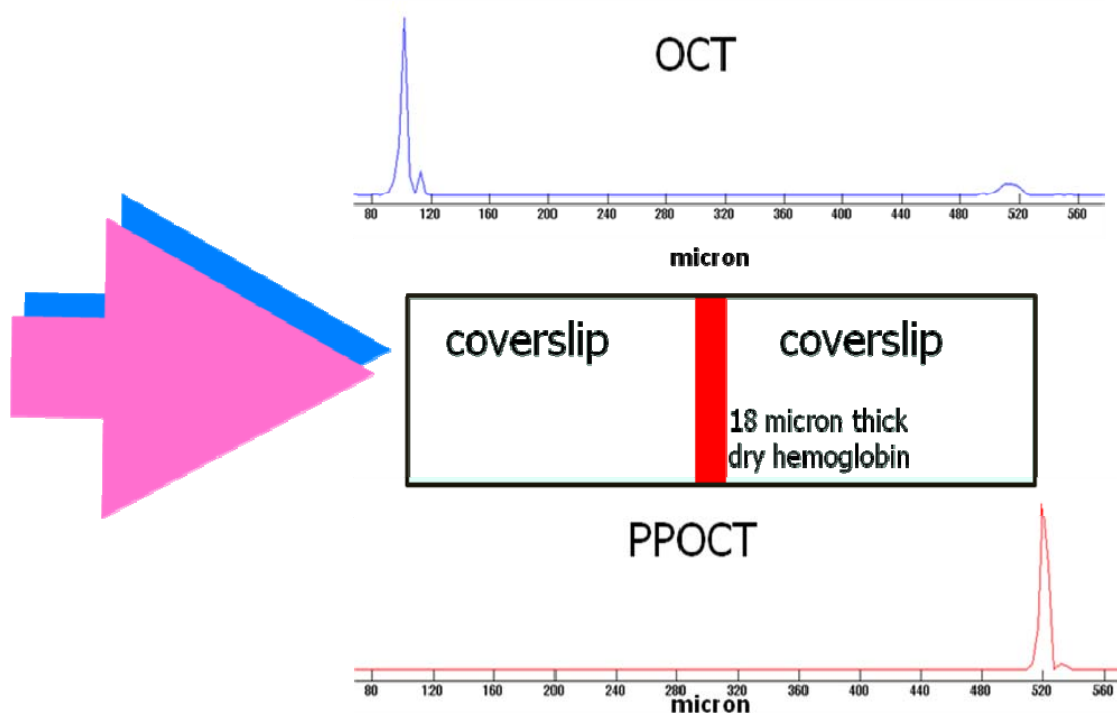

Figure 9: OCT and PPOCT signal from dry hemoglobin sample. Top: OCT A Line of the Sample shown in the middle. Bottom: PPOCT A-Line of the same sample. Both are on linear scales.

The A- lines were recorded with a probe power of 92 µW on the sample and the incident pump power of 2.3 mW. The pump-probe delay time was 280 +/- 40 psec and the pump signal was modulated at 4 KHz by an optical chopper. The PPOCT A-line was extracted by processing an OCT M-scan consisting of 1000 A-lines collected with an integration time of 30 µs resulting in a PPOCT line rate of ~ 16 Hz. In addition to the processing described above, a PPOCT A-line collected with the pump blocked was subtracted from each PPOCT A-line in order to remove contributions from laser intensity noise.

The OCT A-line clearly shows two peaks, one at each of the two air-glass interfaces in the sample. The hemoglobin-glass interface provides a much weaker reflection which is not visible on this scale. The PPOCT A-line on the other hand exhibits one strong peak at the deepest air-glass interface. We attribute this peak to the transient absorption in hemoglobin.

Although the results were encouraging there was a need to further improve the SNR so that it is not susceptible to the laser intensity noise. Modulating the pump beam at a higher frequency was a simple way to moving the filtered PPOCT signal further away from DC. This was done by using an Electro-Optical Modulator for subsequent testing of the system which was done by using melanin as the target chromophore.

A black, human hair sample was used to demonstrate the sensitivity of our PPOCT system to melanin. The hair sample was placed in the sample arm of the PPOCT system. The probe power on the sample was 1.4 mW and the pump power was approximately 2.5 mW. The line rate was 16.13 kHz with 2000 OCT A-lines used to generate one PPOCT A-line. Figure 10A is the measured OCT A-line of the hair sample on a linear scale. The signal at zero delay is residual DC artifact. Figure 10B is the corresponding PPOCT A-line when the pump is on. Figure 10C is the PPOCT A-line when the pump is off. The small residual signal in 9C was attributed to random intensity noise in the laser source at the pump modulation frequency of 7.68 kHz. The absence of the PPOCT signal when the pump beam is off is consistent with transient absorption. We attribute the transient absorption (PPOCT) signal to eumelanin, the most abundant chromophore in our sample. It should be noted that some of the generated signal may be due to a transient photo-thermal effect.
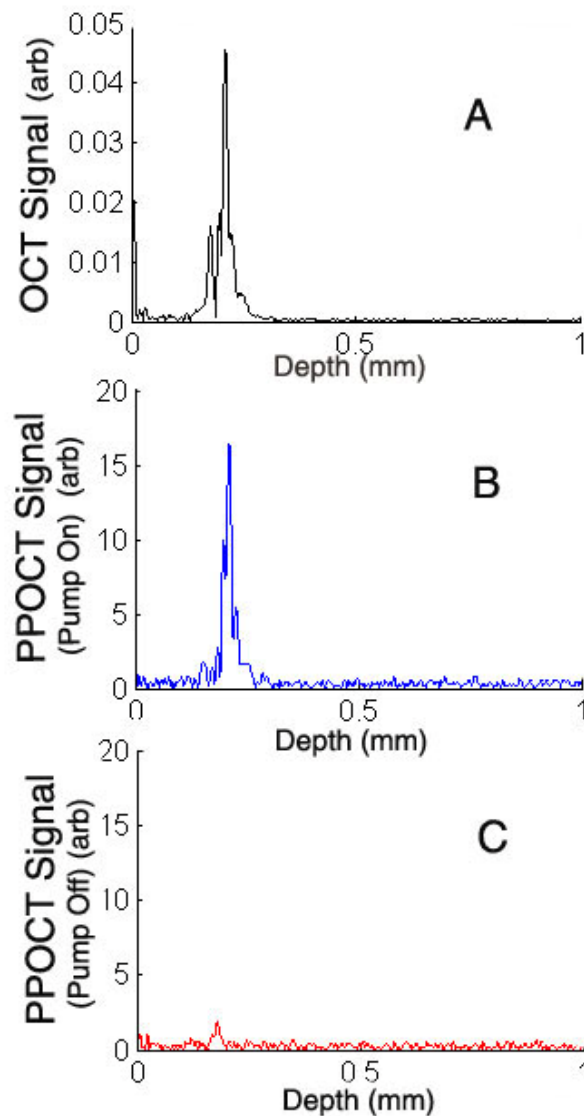
Figure 10: OCT and PPOCT signal from hair. A) OCT A-line from hair sample. B) PPOCT A-line from hair sample with pump on. C) PPOCT A-line from hair with pump off.

We expect that optimization of the pump wavelength and pump probe delay will allow us to improve the SNR and imaging speed to a point where ocular imaging is feasible. One way of improving the SNR is by making the system less susceptible to the

random intensity noise generated by the laser source that contributes to the background signal at the pump modulation frequency. This can be done by collecting the signal at faster rate. This rate is limited by the maximum attainable pump modulation frequency, which, is determined by the Nyquist limit of the line rate (16.13 KHz). Thus the pump-probe signal cannot be sampled at a rate of more than 8.07 KHz.

The line rate can be improved by switching to a faster camera. A camera with 1024 pixels nearly doubles the maximum attainable line rate and in turn the pump modulation frequency limit. A 1024 pixel camera would thus enable us to modulate the pump signal at a frequency of ~13 KHz. This could improve the SNR of the PPOCT signal significantly.

5. CONCLUSION

In conclusion, we have developed a two–color, Fourier domain pump-probe optical coherence tomography system. The system was tested by successfully targeting trans-absorption in specific chromophores such as hemoglobin and melanin. However, while the strong signals obtained from both hemoglobin and melanin are encouraging, we clearly need to continue optimizing the system. One of the areas that we intend to investigate to achieve this goal is reducing the effect of laser intensity noise. We are also looking for means to improve the processing time for the signal by developing a faster algorithm for signal processing.

Working towards these goals, we aim to image liquid hemoglobin in sample vessels that closely simulate microvasculature. This would help us achieve our final objective of mapping the oxygen concentration of the blood and blood flow in microvasculature. We also intend to continue our work on imaging melanin as it is potentially important as a general contrast agent in OCT as well as a clinical tool for the diagnosis and monitoring of melanoma. We expect to optimize the pump wavelength and the pump probe delay that will allow us to improve the SNR and imaging speed to a point where ocular imaging is feasible.

REFERENCES

1. M. E. Fuller, S. H. Streger, R. K. Rothmel, B. J. Mailloux, J. A. Hall, T. C. Onstott, J. K. Fredrickson, D. L. Balkwill and M. F. DeFlaun, "Development of a vital fluorescent staining method for monitoring bacterial transport in subsurface environments," Appl. Environ. Microbiology 66, 4486-4496 (2000).

2. G. B. Yvonne-Tee, A. H. G. Rasool, A. S. Halim and A. R. A. Rahman, "Noninvasive assessment of cutaneous vascular function in vivo using capillaroscopy, plethysmography and laser-Doppler instruments: Its strengths and weaknesses," Clinical Hemorheology and Microcirculation, **34**, 457 (2006).

3. F. S. Laroux and M. B. Grisham, "Immunological basis of inflammatory bowel disease: Role of the microcirculation**,**" Microcirculation, **8**, 283 (Oct, 2001).

4. C. M. Cuthbertson and C. Christophi, "Disturbances of the microcirculation in acute pancreatitis**,**" British Journal of Surgery, **93**, 518 (2006).

5. Z. Haroon, K. Peters, C. Greenberg and M. W. Dewhirst, in *Antiangiogenic agents in cancer therapy*, B. Teicher, Ed. (Totowa, New Jersey, Humana Press, 1998) pp. 3-21.

6. D. Hanahan and J. Folkman, "Patterns and emerging mechanisms of the angiogenic switch during tumorigenesis," Cell, **86**, 353 (1996).

7. N. Ferrara and R. S. Kerbel, "Angiogenesis as a therapeutic target," Nature**, 438**, 967-970, (2005).

8. S. Benz, R. Wiessner, R. Obermaier, F. Pfeffer and U. T. Hopt, "Microcirculatory events in ischemia/reperfusion of the pancreas defined by continuous tissue oximetry," Transpl. Int.**, 15**, 173-179 (2002).

9. M. L. Iabichella, E. Melillo and G. Mosti, "A review of microvascular measurements in wound healing," Int. Journal of Lower Extremity Wounds **5**, 181-199, (2002).

10. J. D. Simon, L. Hong, and D. N. Peles, "Insights into melanosomes and melanin from some interesting spatial and temporal properties," J. Phys. Chem. B, **112**, 13201-13217 (2008).

11. D. Huang, E. A. Swanson, C. P. Lin, J. S. Schuman, W. G. Stinson, W. Chang, M. R. Hee, T. Flotte, K.Gregory and C. A. Puliafito, "Optical coherence tomography," Science, **254**, 1178-1181, (1991).

12. J. A. Izatt, M. D. Kulkarni, H.-W. Wang, K. Kobayashi and M. V. Sivak, "Optical coherence tomography and microscopy in gastrointestinal tissues," IEEE Journal of Selected Topics in Quantum Electronics, **2**, 1017-1028, (1996).

13. G. Häusler and M. W. Lindner, "'Coherence Radar' and 'Spectral Radar'—New tools for dermatological diagnosis," Journal of Biomedical Optics**, 3,** 21-31, (1998).

14. M. Wojtkowski, R. Leitgeb, A. Kowalczyk, T. Bajraszewski and A. F. Fercher, "In vivo human retinal imaging by Fourier domain optical coherence tomography," Journal of Biomedical Optics, **7,** 457-463, (2002).

15. M. Wojtkowski, A. Kowalczyk, R. Leitgeb and A. F. Fercher, "Full range complex spectral optical coherence tomography technique in eye imaging," Opt. Lett., **27**, 1415-1417 (2002).

16. S. R. Chinn, E. A. Swanson and J. G. Fujimoto, "Optical coherence tomography using a frequency-tunable optical source," Opt. Lett., **22**, 340-342, (1997).

17. B. Golubovic, B. E. Bouma, G. J. Tearney and J. G. Fujimoto, "Optical frequency-domain reflectometry using rapid wavelength tuning of a Cr4+:forsterite laser," Opt. Lett., **22**, 1704-1706, (1997).

18. F. Lexer, C. K. Hitzenberger, A. F. Fercher and M. Kulhavy, "Wavelength-tuning interferometry of intraocular distances," Applied Optics-OT, **36**, 6548-6553, (1997).

19. S. H. Yun, G. J. Tearney, J. F. de Boer, N. Iftimia and B. E. Bouma, "High-speed optical frequency-domain imaging," Optics Express, **11**, 2953-2963, (2003).

20. K. D. Rao, M. A. Choma, S. Yazdanfar, A. M. Rollins and J. A. Izatt, "Molecular contrast in optical coherence tomography by use of a pump-probe technique," Opt. Lett., **28**, 340-342 (2003).

21. C. Yang, M. A. Choma, L. E. Lamb, J. D. Simon and J. A. Izatt, "Protein-based molecular contrast optical coherence tomography with phytochrome as the contrast agent," Opt. Lett., **29**, 1396-1398 (2004).

22. B. E. Applegate, C. Yang, A. M. Rollins and J. A. Izatt, "Polarization resolved second harmonic generation optical coherence tomography in collagen," Opt. Lett., **29**, 2252-2254 (2004).

23. Jiang, I. Tomov, Y. Wang and Z. Chen, "Second-harmonic optical coherence tomography," Opt. Lett., **29**, 1090-1092 (2004).

24. M. V. Sarunic, B. E. Applegate and J. A. Izatt, "Spectral domain second harmonic optical coherence tomography," Opt. Lett., **30**, 2391-2393 (2005).

25. J. S. Bredfeldt, C. Vinegoni, D. L. Marks and S. A. Boppart, "Molecularly sensitive optical coherence tomography," Opt. Lett., **30**, 495-497 (2005).

26. C. Yang, L. E. L. McGuckin, J. D. Simon, M. A. Choma, B. E. Applegate and J. A. Izatt, "Spectral triangulation molecular contrast optical coherence tomography with indocyanine green as the contrast agent," Opt. Lett., **29**, 2016-2018 (2004).

27. A. L. Oldenburg, F. J.-J. Toublan, K. S. Suslick, A. Wei and S. A. Boppart, "Magnetomotive contrast for in vivo optical coherence tomography," Opt. Express, **13**, 6597-6614 (2005).

28. T. M. Lee, A. L. Oldenburg, S. Sitafalwalla, D. L. Marks, W. Luo, F. J.-J. Toublan, K. S. Suslick and S. A. Boppart, "Engineered microsphere contrast agents for optical coherence tomography," Opt. Lett., **28**, 1546-1548 (2003).

29. J. Chen, F. Saeki, B. J. Wiley, H. Cang, M. J. Cobb, Z.-Y. Li, L. Au, H. Zhang, M. B. Kimmey, X. D. Li and Y. Xia, "Gold nanocages: Bioconjugation and their potential use as optical imaging contrast agents," Nano Lett., **5**, 473-477 (2005).

30. B. E. Applegate, C. Yang and J. A. Izatt, "Theoretical comparison of the sensitivity of molecular contrast optical coherence tomography techniques," Optics Express, **13**, 8146-8163, (2005).

31. B. E. Applegate and J. A. Izatt, "Molecular imaging of endogenous and exogenous molecular chromophores with ground state recovery pump-probe optical coherence tomography," Optics Express, **14**, 9142 – 9155 (2006).

32. Y. Wang, I. Tomov, J. S. Nelson, Z. Chen, H. Lim and F. Wise, "Low-noise broadband light generation from optical fibers for use in high-resolution optical coherence tomography," Journal for Optics Society of America, **22**, 1492-1499, (2005).

33. http://omlc.ogi.edu/spectra/hemoglobin/index.html.

VITA

Desmond Jacob received his Bachelor of Engineering degree in electronics from The University of Pune, India in 2004. He entered the biomedical engineering program at Texas A&M University in August 2006. His research interests include optical imaging modalities and their application in health care. He plans to complete his doctoral studies and join academia.

Mr. Desmond Jacob may be reached at B/21, Kundalini Co-op. Hsg. Soc., Mukteshwar Ashram road, I. I. T Market, Powai, Mumbai 400076, India. His email is desmondjacob@gmail.com.